Nonlinear Dyn (2011) 65:317–334
DOI 10.1007/s11071-010-9894-0

ORIGINAL PAPER

Mathematical modeling and experimental investigation of an embedded vibro-impact system

R.R. Aguiar · H.I. Weber

Received: 30 June 2010 / Accepted: 15 November 2010 / Published online: 8 December 2010

Abstract The subject of this work is the experimental investigation and the mathematical modeling of the impact force behavior in a vibro-impact system, where a hammer is mounted on a cart that imposes a prescribed displacement. By changing the hammer stiffness and the impact gap it is possible to investigate the impact force behavior under different excitation frequencies. The experimental data will be used to validate the mathematical model. The hammer behavior is studied in more detail using a nonlinear analysis, which shows the various responses of the hammer, such as dynamical jumps, bifurcations and chaos.

Keywords Nonlinear dynamics · Impact · Vibro-impact · Impact oscillator

1 Introduction

Oil well drilling in hard rock formations is still a great challenge for oil companies. Optimal productivity is possible by combining advantages of existing drilling techniques: both rotary and percussive drilling. In conventional rotary drilling, the energy applied in the system (oil well drillstring) comes from the rotary table located at the top of the drillstring. Such energy, supplied to drill the oil well, ends up being wasted by vibration (axial, torsional and bending), friction with borehole walls and heat [1–3]. If part of the energy wasted in vibration could be reinserted into the drilling process, the rate of penetration (ROP) could be increased.

The use of the already existing vibrations in the drillstring [2, 4] (in fact, the axial vibration due to the cutting process) to generate a harmonic load on the bit and an excitation in a steel mass (hammer) which will cause impacts, is the motivation of this work (see Fig. 1). The concept of this hybrid drilling technique is to reintroduced the energy wasted on axial vibration, back into the drilling process, with the use of impacts. The stress waves created by such impacts may be useful to release the system from a stick condition of stick-slip phenomena, as well as generating cracks on the rock formation, increasing the rate of penetration. The axial vibration generated by the bit/rock interaction excites the hammer. When the excitation frequency approaches the mass resonance, impacts on the bit occur, since the hammer displacement is limited by the gap. Therefore, in addition to the rotative penetration, a percussive action takes place due to the impact of the hammer on the bit [5, 6]. The idea of combining a percussive action to rotary drilling is not new, be-

R.R. Aguiar (✉)
COPPE—Department of Mechanical Engineering, Universidade Federal do Rio de Janeiro, P.O. Box 68.503, 21.941.972, Rio de Janeiro, RJ, Brazil
e-mail: aguiar.rr@gmail.com

H.I. Weber
Department of Mechanical Engineering, Pontifical Catholic University of Rio de Janeiro, Rua Marquês de São Vicente 225, 22451-900, Rio de Janeiro, RJ, Brazil

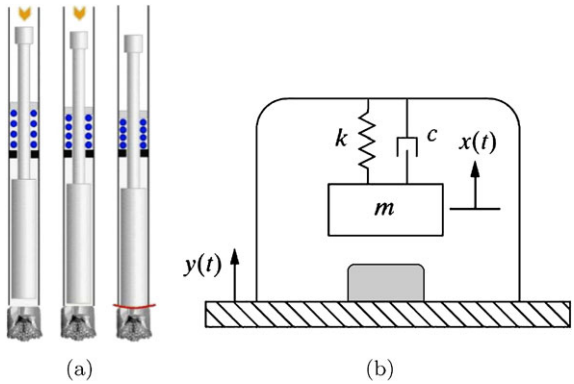

Fig. 1 (**a**) Resonance hammer-drilling technique; (**b**) Embedded vibro-impact system

ing first developed by Hausser and Nüsse & Gräfer in 1955 [5].

The study of vibro-impact systems has been the aim of several researches, from the application of a percussive action in rotary drilling for improved performance [5–7], to ultrasonic drilling [8–10], impact dampers [11, 12] and vibro-safe percussion machines [13].

In general, experimental contributions have been rather limited. Shaw and Holmes [28] experimentally examined the response of a beam with a fixed amplitude constraint at one end, noting that a one-degree-of-freedom approximation allowed prediction of the regions of periodic and chaotic motion. This was extended systematically in Shaw [27], where the subharmonic resonances predicted in Thompson et al. [30] were observed along with period-doubling bifurcations. Ing et al. [29] also studied an impact oscillator with a one-sided elastic constraint. Different bifurcation scenarios have been shown for a number of values of the excitation amplitude, with the excitation frequency as the bifurcation parameter. Various other experimental impact oscillators were studied by Hinrichs et al. [32] and Todd and Virgin [33]. Of note is Piiroinen et al. [31], where a pendulum contacting with a rigid stop was shown to exhibit periodic windows in a period-adding cascade up to period-5.

From the theoretic point of view, vibro-impact system is a quite interesting subject [14] because it presents a rich and complex dynamical response, from periodic to chaotic behavior. Since it is a non-smooth system, bifurcations and other nonlinear phenomena may occur where such behaviors are mostly not present in linear systems. Besides the references mentioned above, several other studies concerning vibro-impact systems are available in the literature, such as the works of Divenyi et al. [20, 21], and Peterka et al. [22–25].

The main objective of this work is to understand the behavior of an impact hammer embedded inside a vibrating structure. The use of new hardware improved the capability of investigating the system in a shorter timescale, enhancing knowledge of contact mechanics. The study of this test rig includes defining its characteristics, like the range of possible excitation frequencies and the measurement of the impulsive forces. The experimental part of this work presents data regarding the vibro-impact system under different hammer characteristics. From the experimental data a mathematical model is proposed and validated. Using numerical simulations the system behavior is investigated in more detail. A nonlinear analysis (bifurcation diagrams, Poincaré maps) is performed, including the mapping of regions of existence and stability of impact motions (called by the authors "Peterka map").

Although the literature shows several studies dealing with vibro-impact systems, as listed, there is little concern regarding the force magnitude developed by the impacts. Since the motivation relies on a hybrid technique to drill hard rock formations, special attention is dedicated in this work regarding this issue, as well as which system parameters combination develops higher impact forces. In this manner, the authors propose a contribution to the field of vibro-impact dynamics: the Peterka map with impact force magnitude addressed. Such a diagram can be used as a design tool for this special type of devices.

2 Experimental apparatus

The experiment consists of a main cart, made of aluminum, which slides along the horizontal axis on a low-friction rail bearing assembly (INA-Laufwagen LFL52-E-SF), see Fig. 2. Excitation is provided by an inverter controlled AC motor (EBERLE model B56b4, 745.7 W). The motor is attached to the cart through a pin that slides into a slot machined on an acrylic plate attached to the cart. The pin hole is drilled off-centered on the disk at the edge of the motor, so that rotational motor movement becomes sinusoidal cart movement. This device is used instead of an electromagnetic shaker because it can perform higher hammer amplitudes than a shaker. The device attempts to

avoid the influence of impact forces on the excitation source.

Hammer mass combines an aluminum coupling that holds the springs and the impact device (steel). Hammer stiffness is assured by two clamped–clamped bending beams (steel). These beams have a transverse section of 22.3 mm width and 0.6 mm height. The length of the beams can be changed in order to vary the hammer stiffness. The length of the beams is defined as the distance between the aluminum couplings (Fig. 3(a)). Different values of the hammer stiffness will be determined by changes in the length of the beams. This information will be used to compare different values of hammer stiffness. To vary the gap between the hammer and the cart, the impact device is composed of a screw and a knurled nut.

The measurement devices on the test rig include:

- one accelerometer attached to the hammer (accelerometer Endevco 751-10 SN AC70);
- one piezoelectric force sensor (PCB 208C03) fixed to the cart and located in front of the hammer impact device;
- two laser displacement sensors, both located on the side of the cart. One of the laser displacement sensors measures cart displacement (optoNCDT 1607-20) and the other measures hammer displacement (optoNCDT 1607-100). Both laser displacement sensors are DC powered (ICEL power supply PS-500).

The accelerometer signal is filtered by a signal conditioner (ENDEVCO Isotron 2792B). The force sensor is powered and its signal filtered by an ICP signal conditioner (PCB 482C05). All data is acquired by two oscilloscopes (Tektronix digital storage oscilloscopes) that use different timescales. The first oscilloscope (TDS 2024B) measures the impact force and acceleration at the precise moment of impact (micro scale), after the impact force signal is triggered. The second oscilloscope (TDS 2012B) measures both cart and hammer displacements using laser displacement sensors signals (macro scale). Sensor specifications are shown in Table 1.

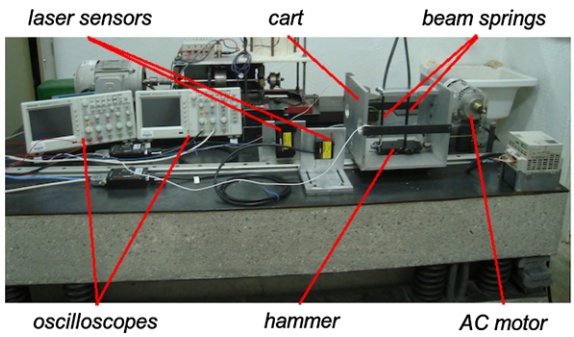

Fig. 2 Test rig

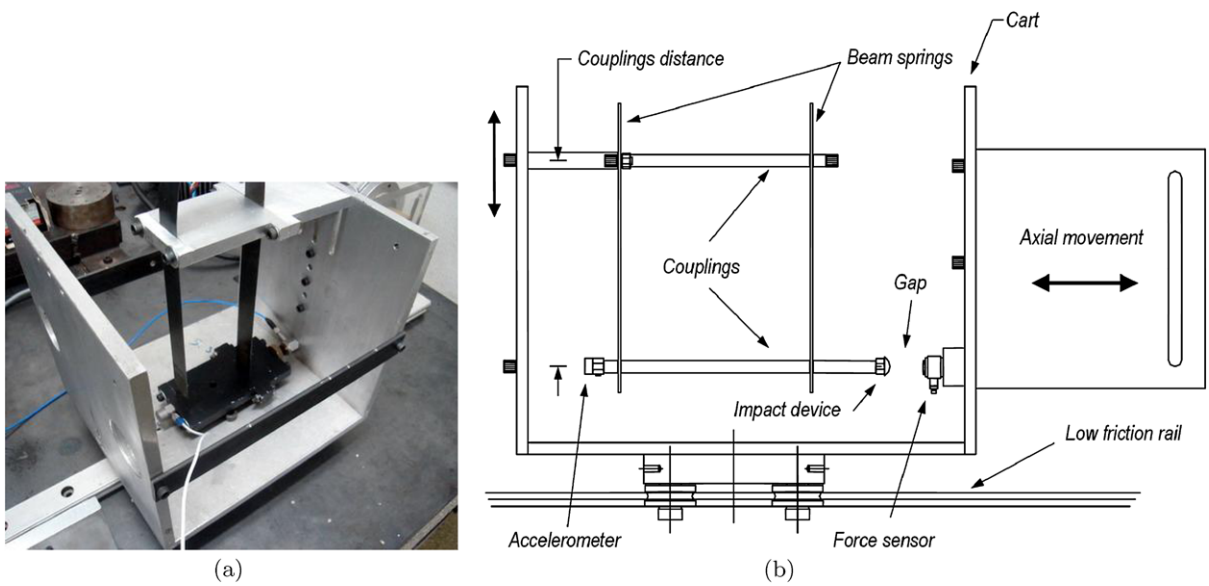

Fig. 3 (**a**) Detail of beam springs supporting the hammer; (**b**) Experimental sketch

Table 1 Sensor specifications

Hammer accelerometer—751-10 SN AC70		
Sensitivity	10.225	mV/g
Measure range	±50	g
Resonance frequency	50	kHz
Impact force sensor—PCB 208C03		
Sensitivity	2.263	mV/N
Measure range	±2.224	kN
Resonance frequency	75	kHz
Cart laser displacement sensor—optoNCDT 1607-20		
Sensitivity	10	V/mm
Measure range	20	mm
Hammer laser displacement sensor—optoNCDT 1607-100		
Sensitivity	2	V/mm
Measure range	100	mm

2.1 Experimental methodology

The test rig considers different values for the impact gap, the hammer stiffness and the excitation frequency. The length of the impact gap is measured using calibrated shims. The excitation frequency is supplied by the AC motor. The system responses are: the hammer acceleration, the impact force, the cart displacement and the hammer displacement.

The methodology is to observe the behavior of the impact system as the values of gap and the hammer stiffness are varied. Three different values for the hammer stiffness (lengths for the beam springs: 170, 150 and 135 mm) and three values for the impact gap: 0.0, 1.0 and 3.0 mm were chosen. The combination generates 9 different possibilities of hammer configurations. For each hammer stiffness, the parameters are identified for the case without impact. Afterwards, a study with impact is carried out. The excitation frequency from the AC motor is varied in order to cover a range of frequencies.

The laser displacement sensor signal presents an undesirable level of noise, which was decreased using a *moving average* filter. The original signal is always compared to the filtered signal, trying to avoid any masking of relevant phenomenon. Due to the nature of the moving average (a low-pass filter), the phase plane charts show a smooth effect during the impact, caused by the differentiation of low-pass filtered signal, as will be seen by the comparison between experimental data and numerical results.

3 Experimental results

3.1 Experimental results for the first value of hammer stiffness (beam spring length 170 mm)

The impact force behavior, as the excitation frequency is swept, can be divided into frequency bands, showing similar characteristics in each frequency band, regardless of the stiffness/gap combination.

Impact gap 0.0 mm For the 0.0 mm gap configuration, the first frequency band is from 4.00 up to 11.50 Hz. This band is characterized by impacts, at one impact per excitation cycle. Defining z, the characteristic of impacts, a fraction where the numerator indicates the amount of impacts and the denominator indicates the excitation cycles. Therefore, for an impact behavior of one impact per one excitation cycle, $z = 1/1$.

At the lowest excitation frequencies (up to 7.00 Hz), the hammer follows the cart movement, with low magnitudes of impact force. As the excitation frequency increases, the magnitude of impact force increases as well, reaching a maximum of 204 N at 9.00 Hz, see Figs. 4 and 5. After reaching this level, the magnitude of the impact force decreases as the excitation frequency increases. Figure 4 shows the behavior of the hammer under the maximum impact force in the frequency band $z = 1/1$ (one impact per one excitation cycle).

From the charts presented in Fig. 4 it can be noticed that impact force transducer captures the first

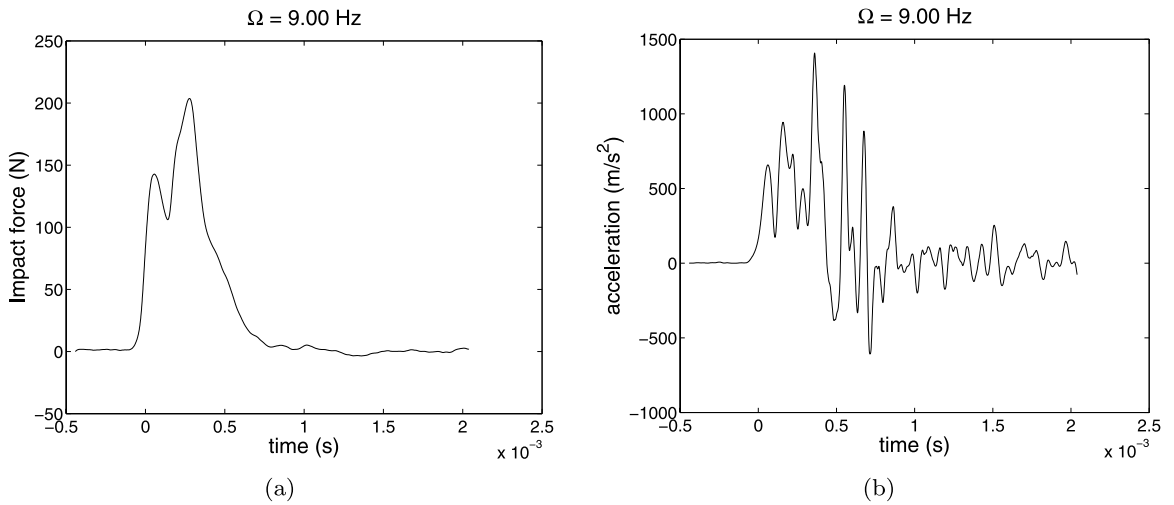

Fig. 4 Couplings distance 170 mm, gap 0.0 mm. Maximum impact force on frequency band $z = 1/1$. Excitation frequency 9.00 Hz: (**a**) Impact force; (**b**) Hammer acceleration

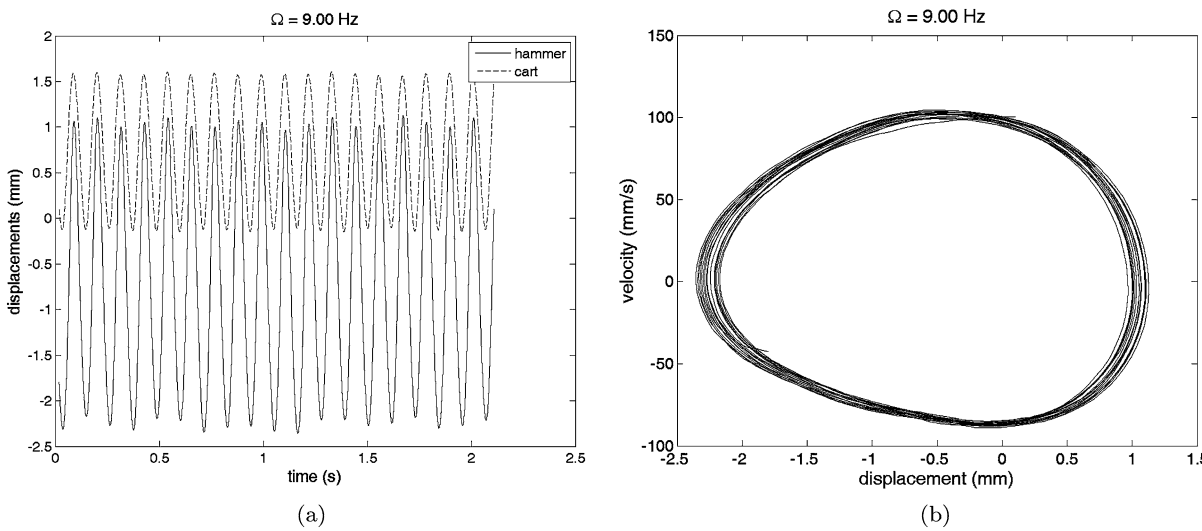

Fig. 5 Couplings distance 170 mm, gap 0.0 mm. Maximum impact force on frequency band $z = 1/1$. Excitation frequency 9.00 Hz: (**a**) Displacements (hammer and cart); (**b**) Hammer phase plane

impulse transferred by the hammer. In a second moment, in this micro scale analysis, the impacted structure will give some impulse back to the hammer, and will react according to an own dynamics originating a second peak. From this chart, observation of experiment and modal analysis of a test rig, it can be concluded that system flexibility is caused by axial vibration of the hammer and bending vibration of the cart plate where the impact force sensor is mounted. Since the hammer is fixed on the opposite side of the knurled nut, the accelerometer measures the hammer dynamics. The existence of contact dynamics is corroborated by the results shown in the acceleration chart, because there are unexpected oscillations after the impact. Further analysis of the test rig, later presented in this work, shows that the peaks in the impact force are caused by bending flexibility of the cart plate where the impact force sensor is mounted. Also, the axial vibration of the hammer is relevant during impact, as shown in the acceleration charts.

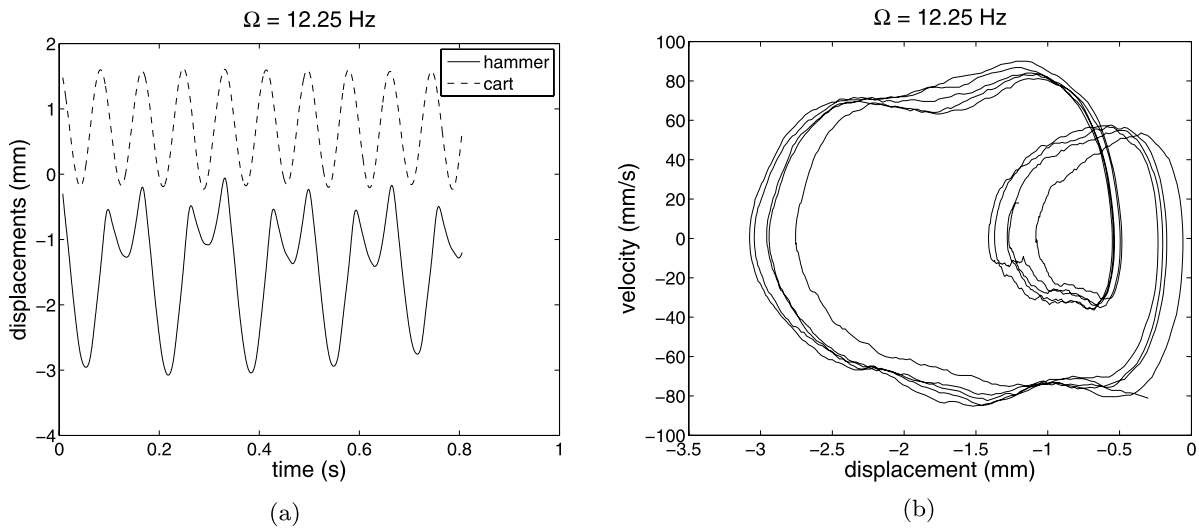

Fig. 6 Couplings distance 170 mm, gap 0.0 mm. Transitory behavior. Excitation frequency 12.25 Hz: (**a**) Displacements; (**b**) Hammer phase plane

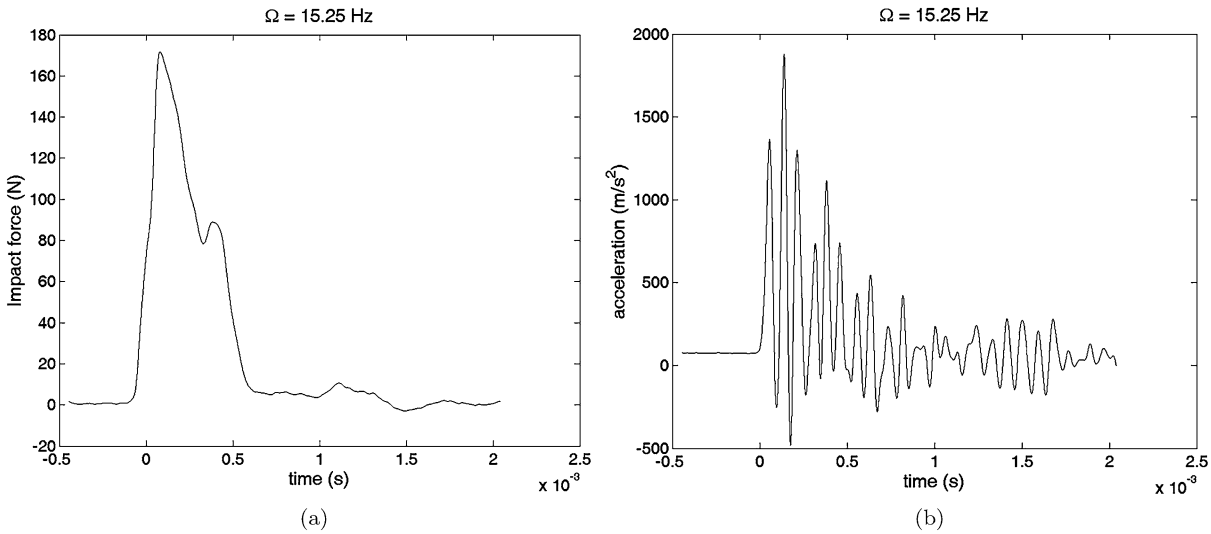

Fig. 7 Couplings distance 170 mm, gap 0.0 mm. Excitation frequency 15.25 Hz, $z = 1/2$: (**a**) Impact force; (**b**) Hammer acceleration during impact

After the first frequency band, the systems goes through a transitory behavior (bifurcation), characterized by a change in impact characteristics. The impact behavior is still at impact per excitation cycle ($z = 1/1$). However, the impacts have alternate magnitudes, as shown in Fig. 6.

In the second frequency band, from 12 to 16 Hz, the impacts occur every two cycles of excitation ($z = 1/2$), see Figs. 7 and 8. Because of high frequencies, the excitation force increases substantially as does the impact force, see (2). Although the maximum impact force at frequency band $z = 1/2$ is higher than at frequency band $z = 1/1$, it is important to remember that at frequency $z = 1/2$ the impacts occur every two cycles and also that energy introduced into the system increases with the square of the excitation frequency. Once the cart displacement is prescribed, as in

$$x_{\text{exc}} = A_0 \cos(\Omega t), \tag{1}$$

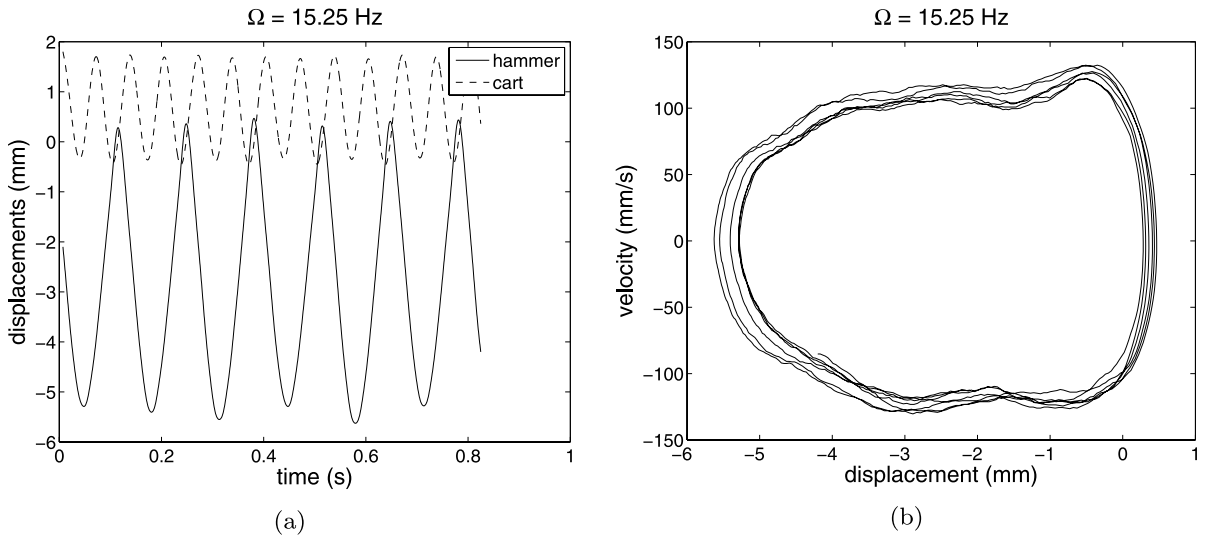

Fig. 8 Couplings distance 170 mm, gap 0.0 mm. Excitation frequency 15.25 Hz, $z = 1/2$: (**a**) Displacements; (**b**) Hammer phase plane

the magnitude of the excitation force F_{exc}, according to Newton's second law, becomes

$$\|F_{\text{exc}}\| = \|M\ddot{x}_{\text{exc}}\| = MA_0\Omega^2, \tag{2}$$

where M is the total mass (cart and hammer combined), A_0 is the displacement amplitude of the cart and Ω is the excitation frequency. Therefore, for a possible field application, the idea is to use the axial vibration of the drillstring to generate the excitation, and this excitation is generally in the low-frequency range, i.e., within the impact force behavior at $z = 1/1$.

At this point it is important to emphasize that excitation is not influenced by the impacts, even in conditions of maximum impact force. This is confirmed by the cart displacement under different excitation frequencies. With this experimental data it is possible to analyze the system behavior in the frequency domain. To do so, a computational routine has been developed to determine the F_i (impact force peak). The maximum value of F_i has been found for each excitation frequency, so this routine masks the hammer behavior if there is a bifurcation in the impact force or a chaotic behavior is present. To generate a non-dimensional chart, the force ratio F_i/mg is used (mg is the hammer weight), and the excitation frequency is divided by the natural frequency of the hammer without impact. The natural frequency of the hammer is experimentally identified using modal analysis. This non-dimensional chart will be useful to compare data between different hammer configurations. For this particular stiffness/gap configuration, the impact force ratio chart (F_i/mg) in the frequency domain is shown in Fig. 9(a).

Using a concept from the linear theory to describe a nonlinear behavior, the excitation frequency where the maximum impact force is achieved is defined as *impact resonance*. Since the hammer displacement is limited by a gap, an interesting phenomenon occurs. The occurrence of the impacts significantly changes the value of the impact resonance, as compared to the hammer resonance. This change of resonance in the occurrence of impacts has already been studied [15] and these results were expected.

Impact gap 1.0 and 3.0 mm Similarly to the results obtained for gap 0.0 mm configuration, the hammer response for 1.0 and 3.0 mm gap configurations may also be separated into frequency bands. Some differences are observed in these non-zero gap conditions as compared to 0.0 mm gap condition. For instance, the occurrence of nonlinear jump after the impact resonance. Another difference is the occurrence of conditions of no impact at higher excitation frequencies. Charts in Fig. 9(b) and (c), show the maximum impact force in the frequency domain, for gaps 1.0 and 3.0 mm, respectively.

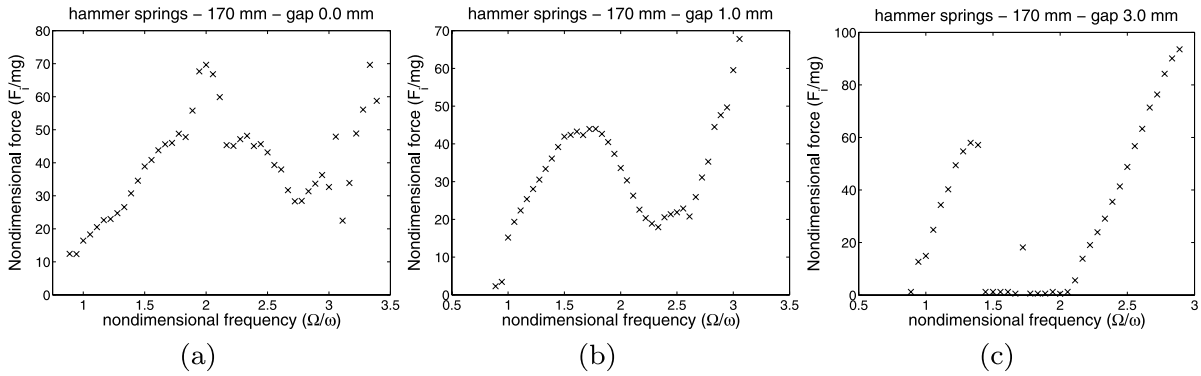

Fig. 9 Frequency domain response, non-dimensional force, F_i/mg: Couplings distance 170 mm: (**a**) gap 0.0 mm; (**b**) gap 1.0 mm; (**c**) gap 3.0 mm

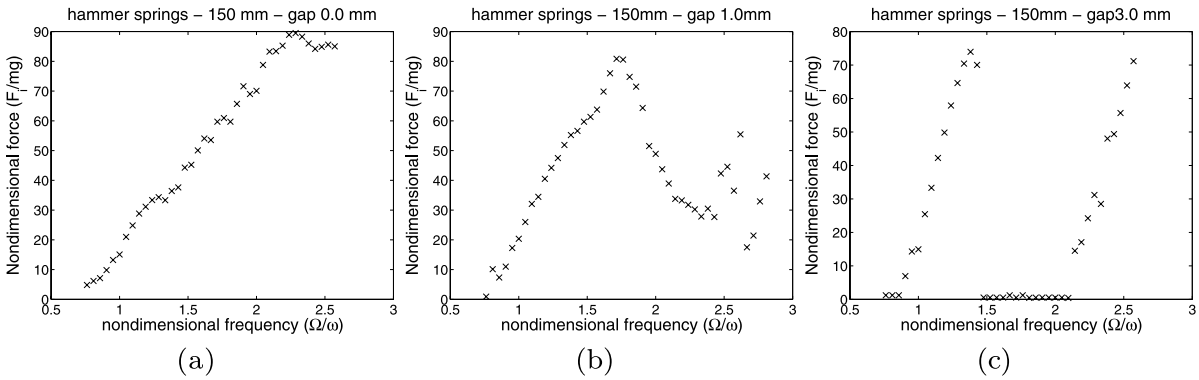

Fig. 10 Frequency domain response, non-dimensional force, F_i/mg: Couplings distance 150 mm: (**a**) gap 0.0 mm; (**b**) gap 1.0 mm; (**c**) gap 3.0 mm

3.2 Experimental results for the second value of hammer stiffness (beam spring length 150 mm)

For this hammer stiffness, the same gaps were used (0.0, 1.0 and 3.0 mm), and the same frequency band pattern was observed. Due to a smaller beam spring length (consequently a higher value of hammer stiffness), higher impact resonance frequencies are found for each stiffness/gap configuration. The test rig shows a limitation at higher excitation frequencies. When the excitation frequency reaches 12 Hz or more, the vibration levels on the mounting structure supporting the AC motor become substantially higher. This vibration level is transmitted to the rest of the test rig (low-friction rail, cart and hammer). Charts in Fig. 10 show the maximum impact force in the frequency domain, for gaps 0.0, 1.0 and 3.0 mm, respectively.

3.3 Experimental results for the third value of hammer stiffness (beam spring length 135 mm)

The impact force behavior of this hammer stiffness follows the same patterns already observed, regardless of the gap imposed. For the 0.0 mm gap configuration, it was not possible to identify the impact resonance frequency ($z = 1/1$), because the frequency was out of the test rig range measuring capability. For the other gap configurations, 1.0 and 3.0 mm, the impact resonance frequency was observed. No data at frequency band $z = 1/2$ was obtained due to test rig limitation. The nonlinear jump after the impact resonance was observed for the 3.0 mm gap configuration but it was not observed for the 1.0 mm gap.

Because the impact force pattern is similar to previous experiments, charts documenting the outputs are

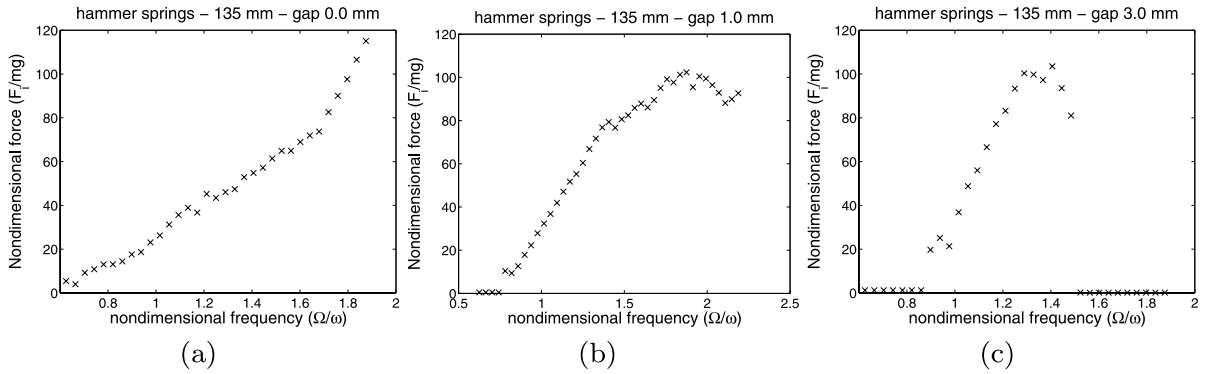

Fig. 11 Frequency domain response, non-dimensional force, F_i/mg: Couplings distance 135 mm: (**a**) gap 0.0 mm; (**b**) gap 1.0 mm; (**c**) gap 3.0 mm

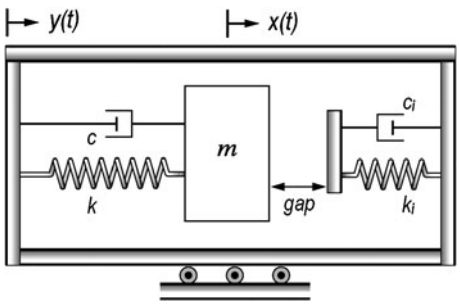

Fig. 12 Mathematical modeling, physical representation

omitted. Figure 11 shows the non-dimensional force in the frequency domain for all gap configurations.

4 Mathematical modeling and comparison between numerical simulation and experimental results

The mathematical modeling of this test rig is presented below. A simple mass–spring–damper system with base excitation [16] is used. The clamped-clamped beam springs' behavior is modeled as nonlinear spring (cubic). See Fig. 12.

For the situation of no impact, i.e. $x - (y + gap) > 0$, equation of motion is

$$m\ddot{x} + c\dot{x} + k\left(x + x^3\right) = F = c\dot{y} + k\left(y + y^3\right), \tag{3}$$

where

$$\begin{aligned} y &= A_0 \sin(\Omega t), \\ \dot{y} &= A_0 \Omega \cos(\Omega t). \end{aligned} \tag{4}$$

The impact model used is the spring-dashpot model [17]. Figure 13 shows one comparison between experimental data and numerical simulation for the case where the cart is not moving and the hammer is released from a known initial condition. This result was used to identify the impact parameters.

Although the spring-dashpot model is not capable of reproducing the real impact force profile over time due to the jump caused by the damping force, this model generated satisfactory results. Impact parameters for this model are listed in Table 2.

Therefore, when the hammer is impacting the cart $(x - (y + gap) \leqslant 0)$, the equation of motion will change to

$$\begin{aligned} &m\ddot{x} + c\dot{x} + k\left(x + x^3\right) = F - F_i, \\ &F_i = k_i\delta + c_i\dot{\delta}, \end{aligned} \tag{5}$$

where the penetration δ and the velocity of penetration $\dot{\delta}$ are described as

$$\begin{aligned} \delta &= x - (y + gap), \\ \dot{\delta} &= \dot{x} - \dot{y}. \end{aligned} \tag{6}$$

Model parameters are shown in Table 3.

According to the Filippov theory [18, 19], the mathematical modeling presented is described by a differential equation with a discontinuous right-hand side. Therefore, the state space $\dot{\mathbf{x}} = f(\mathbf{x}), \mathbf{x} \in \mathbf{R}^n$ may be split into two subspaces Γ_- and Γ_+, separated by a hyper-surface Σ. Hyper-surface is defined by a scalar function $h(\mathbf{x})$. Consequently, the state space $\mathbf{x}$ is in Σ when $h(\mathbf{x}) = 0$. Hence, it is possible to define the subspaces Γ_- and Γ_+, as well as the hyper-surface Σ,

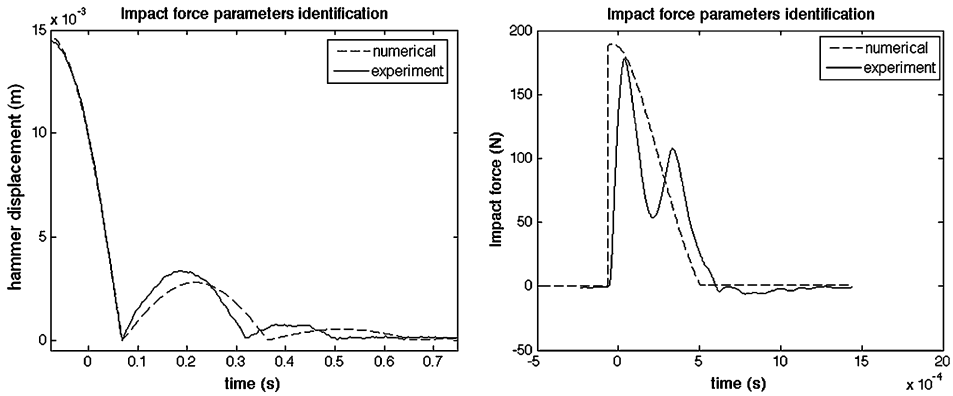

Fig. 13 Impact force parameters identification. Comparison between experimental data and numerical simulation. Impact modeled using the spring-dashpot model

Table 2 Impact parameters: spring-dashpot model

Parameter	Value	Unit
Impact stiffness, k_i	$5.5 \cdot 10^6$	N/m
Impact damping, c_i	$1.2 \cdot 10^3$	Ns/m

using the sets:

$$\begin{aligned} \Gamma_- &= \{\mathbf{x} \in \mathbf{R}^n \mid h(\mathbf{x}) < 0\}, \\ \Sigma &= \{\mathbf{x} \in \mathbf{R}^n \mid h(\mathbf{x}) = 0\}, \\ \Gamma_+ &= \{\mathbf{x} \in \mathbf{R}^n \mid h(\mathbf{x}) > 0\}. \end{aligned} \tag{7}$$

Some physical systems need different interfaces in order to perform a correct description of the transitions. The impact force model used in the mathematical modeling is an example. Due to the nature of the impact model, the contact between the mass and the support occurs whenever the linear displacement becomes equal to the contact gap. However, the mass loses contact with the support when the contact force vanishes. Two indicator functions are used to define the system subspaces (more detail on this mathematical procedure can be found in the works of Divenyi et al. [20, 21]):

$$\begin{aligned} h_\alpha(\theta, \dot{\theta}) &= l \sin\theta - gap, \\ h_\beta(\theta, \dot{\theta}) &= k_i \delta + c_i \dot{\delta}, \end{aligned} \tag{8}$$

where the penetration δ and velocity of penetration $\dot{\delta}$ are already defined in (6).

Table 3 Hammer supported by beam springs: parameters identification

Parameter	Value	Unit
Hammer mass, m	0.298	kg
Cart mass, M	5.38	kg
Excitation amplitude, A_0	0.89	mm
Damping ratio, ζ	0.004	
Couplings distance	Value	Unit
170 mm		
Natural frequency, ω	4.50	Hz
Damping coefficient, ζ	0.06	Ns/m
Couplings distance	Value	Unit
150 mm		
Natural frequency, ω	5.25	Hz
Damping coefficient, ζ	0.08	Ns/m
Couplings distance	Value	Unit
135 mm		
Natural frequency, ω	6.50	Hz
Damping coefficient, ζ	0.09	Ns/m

The mass is not in contact with the support if the state vector $\mathbf{x} = (\theta, \dot{\theta}) \in \Gamma_-$, in other words:

$$\Gamma_- = \{\mathbf{x} \in \mathbf{R}^2 \mid h_\alpha(\theta, \dot{\theta}) < 0 \text{ or } h_\beta(\theta, \dot{\theta}) < 0\}. \tag{9}$$

For the case when there is a contact between the mass and the support:

$$\Gamma_+ = \{\mathbf{x} \in \mathbf{R}^2 \mid h_\alpha(\theta, \dot{\theta}) > 0 \text{ and } h_\beta(\theta, \dot{\theta}) > 0\}. \tag{10}$$

The hyper-surface Σ consists of the conjunction of two surfaces, Σ_α and Σ_β. The hyper-surface Σ_α defines the transition from Γ_- to Γ_+, i.e., when the mass initiates the contact with the support,

$$\Sigma_\alpha = \left\{\mathbf{x} \in \mathbf{R}^2 \;\middle|\; h_\alpha(\theta, \dot{\theta}) = 0 \text{ and } h_\beta(\theta, \dot{\theta}) \geqslant 0\right\}. \quad (11)$$

Surface Σ_β defines the transition from Γ_+ to Γ_- as the contact is lost when the impact force vanishes:

$$\Sigma_\beta = \left\{\mathbf{x} \in \mathbf{R}^2 \;\middle|\; h_\alpha(\theta, \dot{\theta}) \geqslant 0 \text{ and } h_\beta(\theta, \dot{\theta}) = 0\right\}. \quad (12)$$

Consequently, the state equation of this discontinuous system is written as follows:

$$\dot{\mathbf{x}} = f(\mathbf{x}, t) = \begin{cases} f_-(\mathbf{x}, t), & \mathbf{x} \in \Gamma_-, \\ \overline{co}\{f_-(\mathbf{x}, t), f_+(\mathbf{x}, t)\}, & \mathbf{x} \in \Sigma, \\ f_+(\mathbf{x}, t), & \mathbf{x} \in \Gamma_+, \end{cases} \quad (13)$$

where

$$f_-(\mathbf{x}, t) = \begin{bmatrix} \dot{x} \\ \frac{1}{m}(-c(\dot{x} - \dot{y}) - k(x - y) - k(x - y)^3) \end{bmatrix}; \quad \mathbf{x} \in \Gamma_- \quad (14)$$

$$f_+(\mathbf{x}, t) = \begin{bmatrix} \dot{x} \\ In\frac{1}{m}(-c(\dot{x} - \dot{y}) - k(x - y) - k(x - y)^3 - F_i) \end{bmatrix}; \quad \mathbf{x} \in \Gamma_+ \quad (15)$$

$$\overline{co}\left\{f_-(\mathbf{x}, t), f_+(\mathbf{x}, t)\right\} = \begin{bmatrix} \dot{x} \\ \frac{1}{m}(-c(\dot{x} - \dot{y}) - k(x - y) - k(x - y)^3 - (c_i\dot{\delta})) \end{bmatrix}; \quad \text{in } \Sigma_\alpha \quad (16)$$

$$\overline{co}\left\{f_-(\mathbf{x}, t), f_+(\mathbf{x}, t)\right\} = \begin{bmatrix} \dot{x} \\ \frac{1}{m}(-c(\dot{x} - \dot{y}) - k(x - y) - k(x - y)^3) \end{bmatrix}; \quad \text{in } \Sigma_\beta. \quad (17)$$

This approach allows one to numerically integrate non-smooth systems [20].

4.1 Comparison between numerical simulation and experimental results

The comparison between numerical simulation and experimental results starts with the chart of the non-dimensional force (F_i/mg) in the frequency domain (Ω/ω), for each stiffness and gap imposed on the test rig. These results are shown in Figs. 14, 15 and 16. The methodology applied in order to identify the impact force is the same performed for the experimental data, where for each excitation frequency the maximum impact force is detected, regardless of the impact force behavior.

Simulation results show satisfactory agreement with the experimental data. For the beam springs of length 170 mm, Fig. 14, the simulation captures well the maximum impact force and also the presence of the nonlinear jump, for the 3.0 mm gap configuration (Fig. 14(c)).

For the beam spring of length 150 mm, the agreement is better for the 1.0 mm gap configuration. For the 0.0 mm gap configuration, the agreement is satisfactory until the excitation frequency is twice the value of the natural frequency of the hammer. For the 3.0 mm gap configuration, agreement is also satisfactory, although the nonlinear jump is detected with a 10% error in frequency.

For the beam spring of length 135 mm, the agreement is satisfactory up to a non-dimensional frequency of 1.7, for the cases of 0.0 and 1.0 mm gap.

4.2 Nonlinear analysis: bifurcation diagrams, Peterka map and basins of attraction

In this subsection, some nonlinear tools are used to investigate the hammer behavior, starting with the bifurcation diagrams, shown in Figs. 17, 18 and 19.

Two interesting issues can be observed. First, the bifurcation diagrams of the experimental data in all stiffness/gap combinations present a group of dispersed points, even in regions where a steady behavior was observed (for example, $z = 1/1$). The second observation is related to the disagreement between numerical simulation and experiment data. The simulation results present higher amplitudes than the experimental data. The phenomenon that justifies both issues is the energy distribution in the bending vibration modes of the beam springs after each impact. This can be shown obtaining the experimental modal analysis

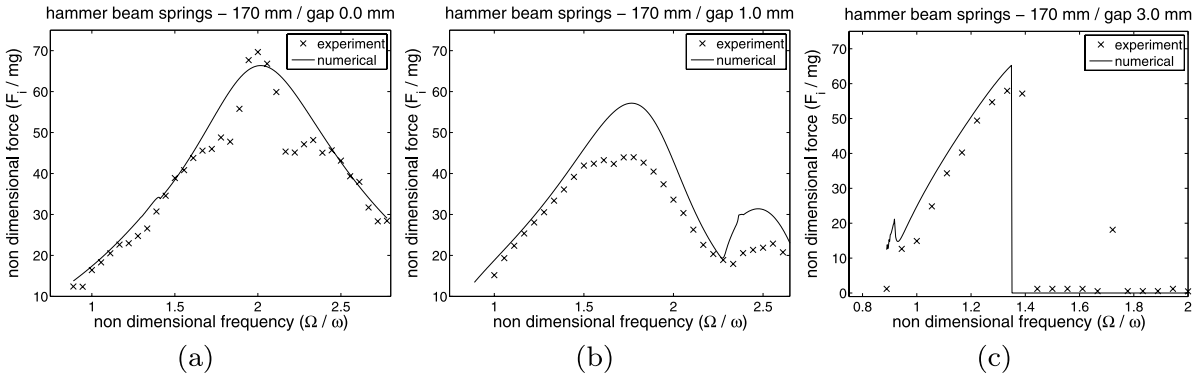

Fig. 14 Numerical/experiment comparison; non-dimensional force *versus* non-dimensional frequency. Couplings distance 170 mm: (**a**) gap 0.0 mm; (**b**) gap 1.0 mm; (**c**) gap 3 mm

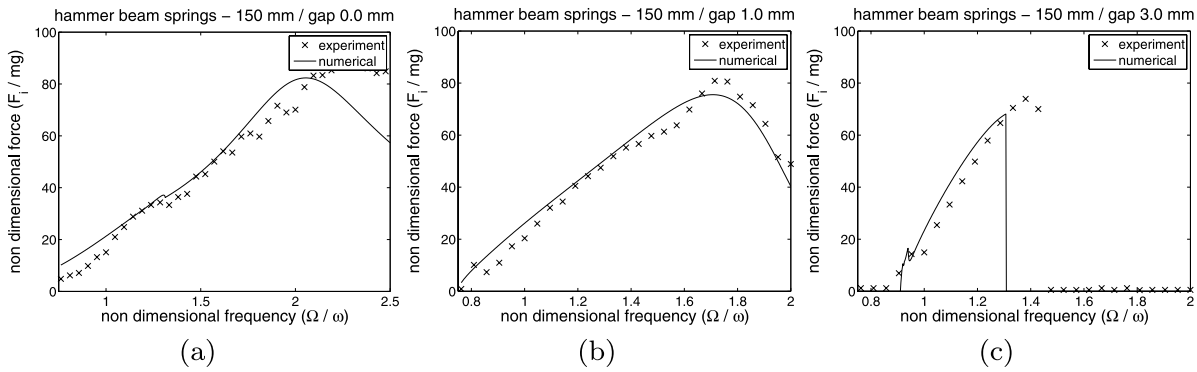

Fig. 15 Numerical/experiment comparison; non-dimensional force *versus* non-dimensional frequency. Couplings distance 150 mm: (**a**) gap 0.0 mm; (**b**) gap 1.0 mm; (**c**) gap 3 mm

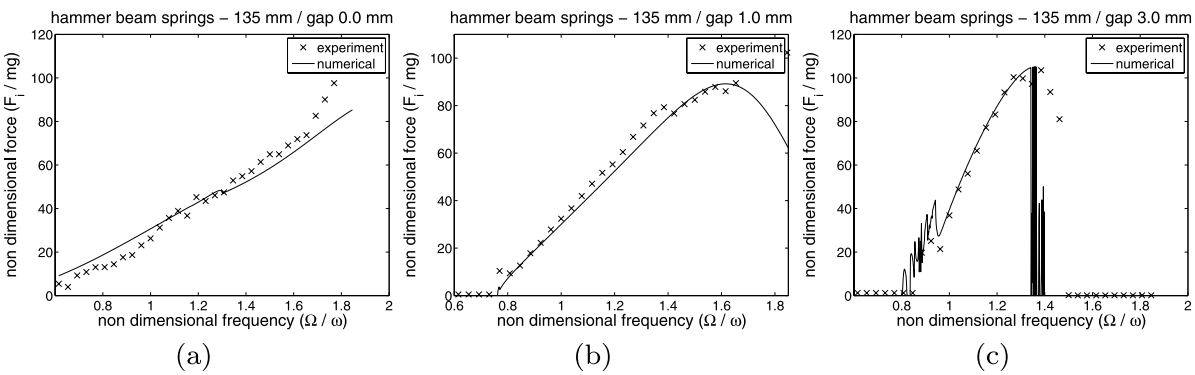

Fig. 16 Numerical/experiment comparison; non-dimensional force *versus* non-dimensional frequency. Couplings distance 135 mm: (**a**) gap 0.0 mm; (**b**) gap 1.0 mm; (**c**) gap 3 mm

of the beam springs right after the instant of impact. The frequency response of the bending beams after the impact is shown in Fig. 20.

To better understand the hammer dynamics, a modal analysis is performed, where the natural frequencies of the hammer with the beam springs are determined. The

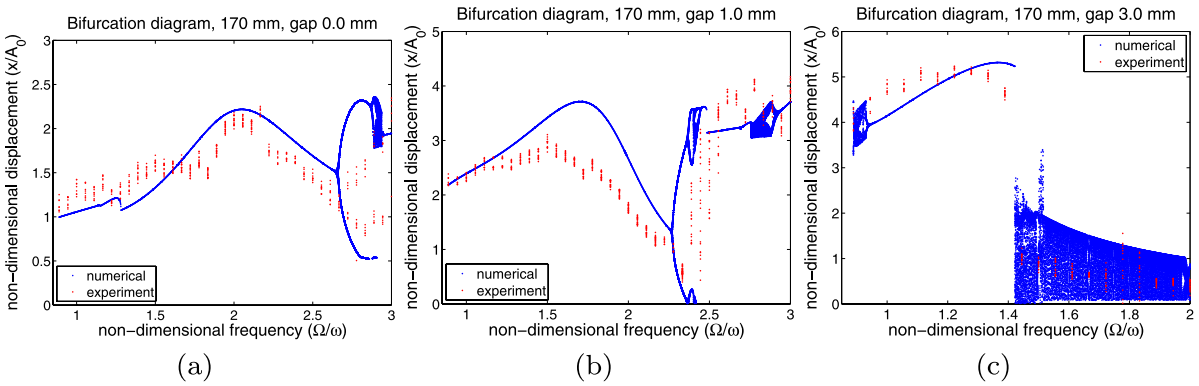

Fig. 17 (Color online) Bifurcation diagrams, hammer displacement, numerical simulation (*blue*)/experimental data (*red*) comparison. Couplings distance 170 mm: (**a**) gap 0.0 mm; (**b**) gap 1.0 mm; (**c**) gap 3.0 mm

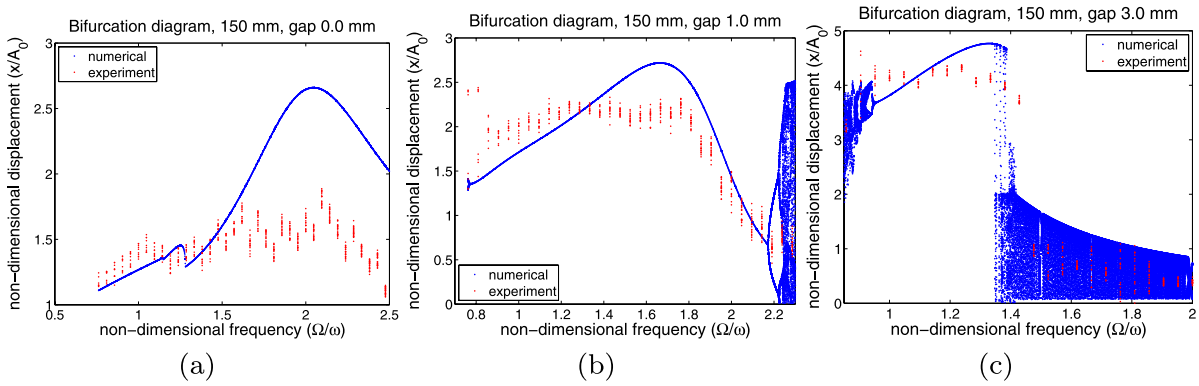

Fig. 18 (Color online) Bifurcation diagrams, hammer displacement, numerical simulation (*blue*)/experimental data (*red*) comparison. Couplings distance 150 mm: (**a**) gap 0.0 mm; (**b**) gap 1.0 mm; (**c**) gap 3.0 mm

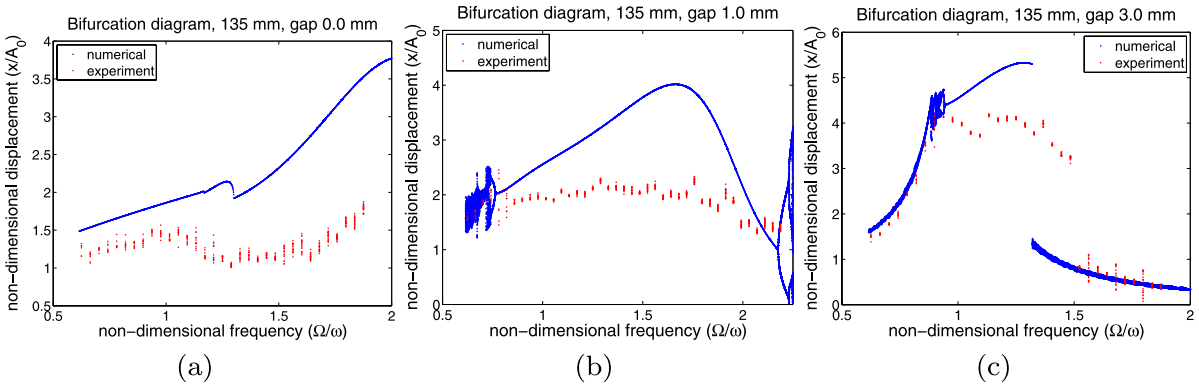

Fig. 19 (Color online) Bifurcation diagrams, hammer displacement, numerical simulation (*blue*)/experimental data (*red*) comparison. Couplings distance 135 mm: (**a**) gap 0.0 mm; (**b**) gap 1.0 mm; (**c**) gap 3.0 mm

experiment is equipped with an extra mini accelerometer (Endevco 25B, SN BL55, sensitivity 4.7707 mv/g), located on one of the beam springs at the end closest to the hammer. The idea is to separate the frequency response function of the hammer from the beam springs. The impact force signal is used as the trigger and the

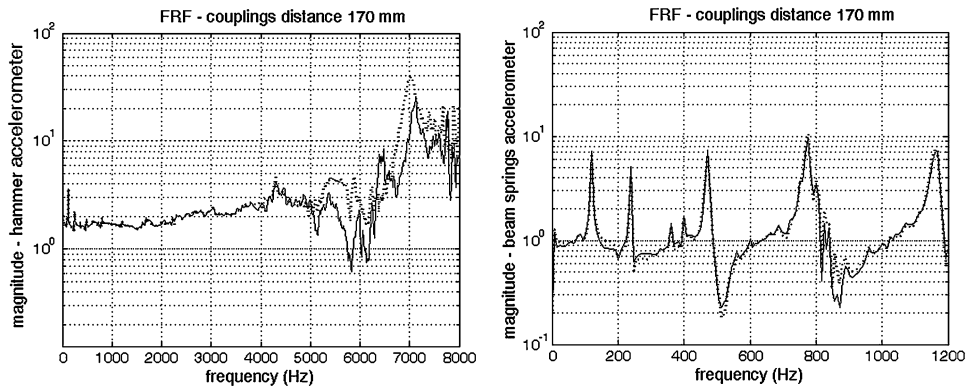

(a) (b)

Fig. 20 Frequency domain response in free flight after impact. Couplings distance 170 mm: (**a**) Hammer accelerometer; (**b**) Beam spring accelerometer

FRF is obtained during the hammer motion following the impact. Two separate tests are performed. For each test the triggered signal is obtained by averaging data from 5 trials. Results are shown in Fig. 20, for beam spring lengths of 170 mm.

After impact the beam springs behave like a clamped–clamped beam in bending vibration. Analyzing the FRFs, several peaks in the low-frequency range are observed. These frequencies are associated with the first bending vibration modes of the beam springs. Also, a peak in the high frequency range is detected (around 7 kHz). This frequency is associated with the axial vibration of the hammer itself.

To understand the hammer axial behavior, the FFT of the hammer acceleration signal during impact was obtained. Several trials were performed and the results are shown in Fig. 21.

The Fourier Transform of the hammer acceleration following impact reveals three peaks shown in Fig. 21. The first peak, in the 1 kHz range, can be associated with the envelope of the acceleration signal. The second peak at around 3 kHz has a lower magnitude and is associated with the impact force profile. The last peak occurs at around 6 kHz and corresponds to the hammer axial oscillations after impact.

The modal analysis shows that after each impact the energy applied to the beam springs is distributed among its bending vibration modes. In the bifurcation map, this energy distribution is shown as a dispersion of the experimental points, even in a steady-state condition. Because the mathematical model considers only the first bending vibration mode, the amplitude obtained by numerical simulation is always higher than the experimental data, even when the impact force is presenting equivalent values. This difference appears to be higher as the stiffness of beam springs increases. Even taken into account this amplitude difference, the transition between frequency bands can be qualitatively observed.

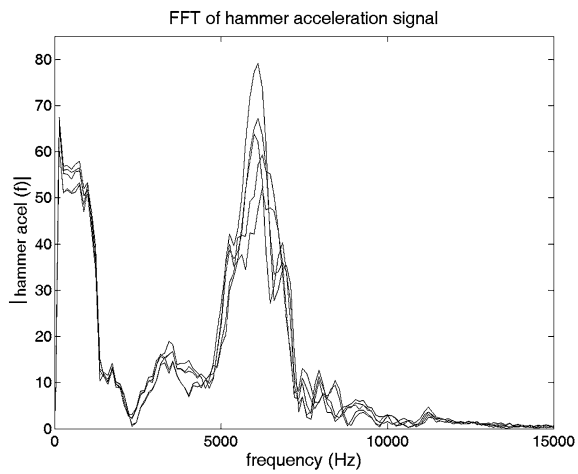

Fig. 21 FFT of several acceleration signals at moment of impact

Although the impact force charts shown in Fig. 17 give some important information regarding the impact force amplitude and the impact resonance, such charts provide neither information about the characteristics of the impact force, nor details on the transition between frequency bands. To better visualize the behavior of this dynamical system, a nonlinear tool is

used. The tool shows a map of regions of stable impact behavior, which the authors call a "Peterka map" [22–25], shown in Fig. 22, which provides information about the characteristic of the impact force as the gap is varied and the range of excitation frequencies is covered. From this chart one can see the areas where the two frequency bands occur, as noted by the red ($z = 1/1$) and green ($z = 1/2$) areas.

The maps are identical for all the cases. This is an indication that the impact force behavior is somehow not dependent on the hammer stiffness. Independence is not completely due to the non-dimensional gap, which takes into consideration the hammer's first natural bending vibration frequency, a function of the system stiffness.

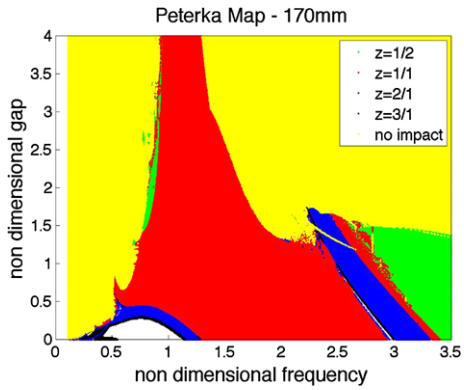

Fig. 22 Peterka map, couplings distance 170 mm

Although the map of regions of stable impact behavior (Peterka map) provides important information about the condition of impact, no information regarding the impact magnitude is given. To overcome this problem, a slight variance of the Peterka map is suggested. The relevant impact condition is $z = 1/1$. Therefore, just this area in the Peterka map is addressed. For each stiffness (addressed as the beam spring length, as mentioned previously), the impact force magnitude is obtained and plotted in colors, see Fig. 23.

This chart provides several important facts about the system behavior and it confirms some aspects observed during the experimental analysis. First, it confirms that the impact force when the hammer is excited in its natural frequency generates impact forces that are 3 times smaller in magnitude than the maximum force. It also shows that the maximum impact force for each given gap does not occur at the $z = 1/1$ boundary, except for high values of gap. Finally, the chart confirms the recommendation to operate in the field using the 0.0 mm gap, because the magnitude of the impact force is in the same value as the impact force in higher gap values. In addition, non-zero gap values are known to present nonlinear jumps.

Finally, the presence of impact and the gap between the hammer and the cart induces nonlinearities, and therefore nonlinear phenomena arise, specifically in the transition between frequency bands. One of these phenomena is the change of the basins of attraction [26] for some gap conditions. In the Peterka

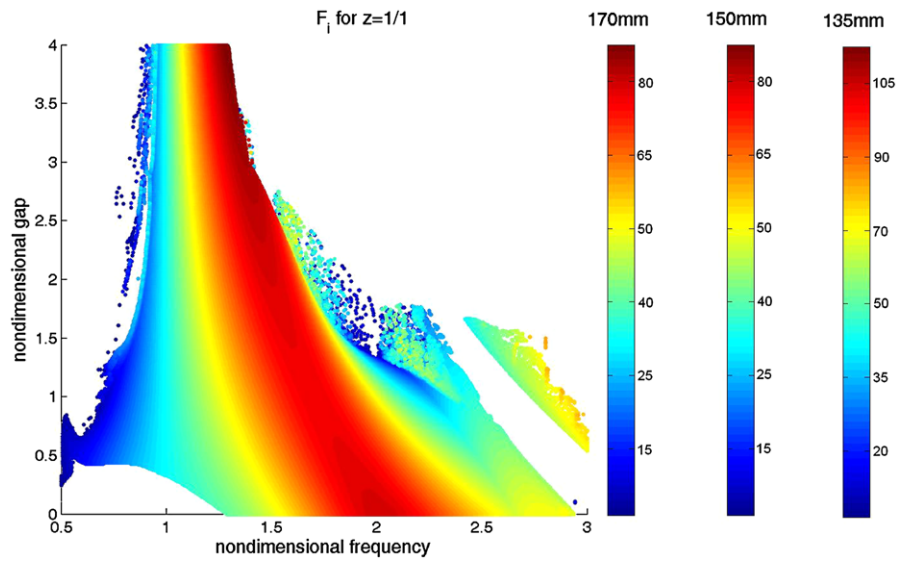

Fig. 23 Peterka map of $z = 1/1$ with impact force magnitude addressed

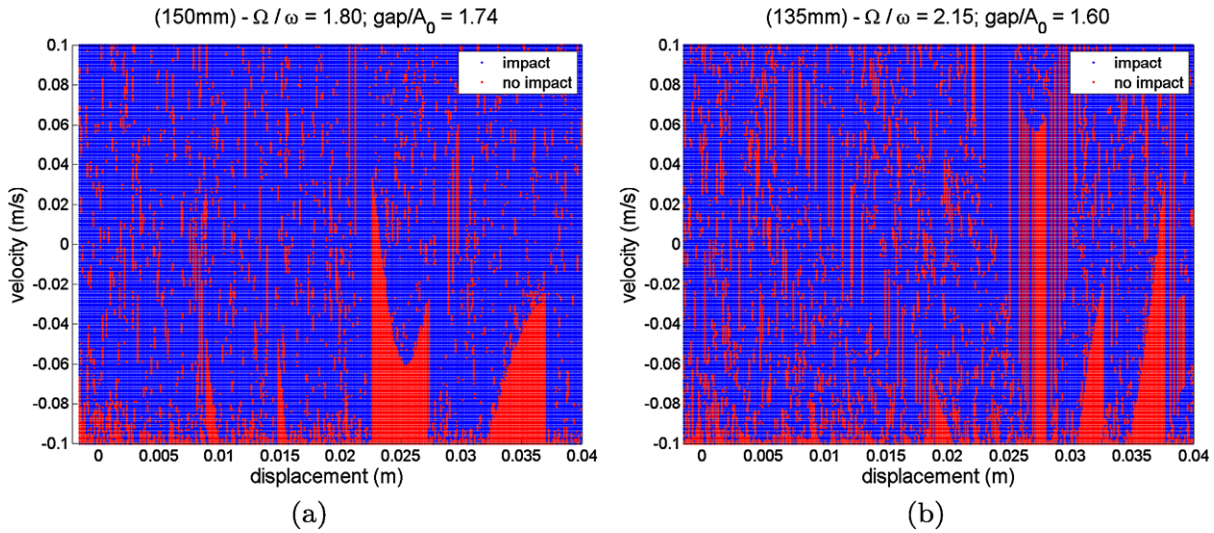

Fig. 24 (Color online) Basins of attraction; condition of impact (*blue*)/no impact (*red*): (**a**) Couplings distance 150 mm, $\Omega/\omega = 1.80$, $gap/A_0 = 1.74$; (**b**) Couplings distance 135 mm, $\Omega/\omega = 2.15$, $gap/A_0 = 1.60$

map, Fig. 22(a)–(c), for a gap condition higher than 1.5, there is an area between the $z = 1/1$ (red) and $z = 1/2$ (green) regions that is characterized by various impact conditions, which are dependent on initial condition of the system.

This area in the Peterka map can be better visualized as a change in the basins of attraction [26], defined as the set of initial conditions $\mathbf{x}_0$ such that $\mathbf{x}(t) \to \mathbf{x}^*$ as $t \to \infty$. See Fig. 24.

5 Conclusions

This work presents results of an experimental investigation and the corresponding mathematical modeling to validate the impact force behavior in a vibro-impact system, where an elastically mounted hammer impacts inside a cart that vibrates under a prescribed displacement. The underlying idea is to use the existing energy in the cart motion to generate impulses which may be useful to the system.

By changing the hammer parameters the impact force behavior is investigated for cart frequencies in a given range. A certain behavior pattern of the impact force is observed allowing the definition of frequency bands presenting similar characteristics according to the gap imposed between the neutral position of the hammer and the impact point on the cart. Inside the bands the impact force behavior presents a regular pattern while in the transition regions between adjacent bands the hammer shows a nonlinear behavior, as basins of attraction, jump phenomena and even chaotic behavior.

The presence of gap significantly changes the frequency where the maximum impact force occurs (called by the authors *impact resonance*) and differs from the hammer's natural frequency. A smoothing effect, which does not reflect the reality of the impact, was noticed in the phase plane charts during impact and is caused by the differentiation of a low-pass filtered signal. To evaluate the influence of the flexibility in the mounting of the hammer [34], its behavior was compared to a situation where the suspension was done using a set of wires which guarantee a parallel displacement of the hammer: it was noted that the elastic suspension leads to significantly higher impact forces, regardless of the stiffness imposed by the beam springs of the hammer suspension.

The mathematical model developed to validate the experiments is capable of determining qualitatively the frequency bands and predicting the impact force magnitude in the frequency domain for each stiffness/gap combination. However, the mathematical model did not predict well the hammer displacement, due to the energy used in the bending vibration modes of the beam springs, which support the hammer, following each impact. This energy distribution can be observed due to the dispersion of the experimental points in

the bifurcation map, even in a steady-state condition. Since the mathematical model considers only the first bending vibration mode, the resulting amplitude is always higher than the one obtained with the experimental data, even when the impact force presents equivalent values. This difference appears to be greater when the beam springs stiffness increases. Another observed aspect is the similarity in the shape pattern of the Peterka maps regardless the value for hammer stiffness, except in the chaotic region between frequency bands $z = 1/1$ (one impact per one excitation cycle) and $z = 1/2$ (one impact every two excitation cycles). This is an indication that the impact force behavior is somehow independent on the hammer stiffness.

Also, a new methodology was proposed to better visualize each impact force behavior in the Peterka map, plotting one impact force characteristic at a time and adding colors to the third coordinate F_i. This methodology provided important information regarding the hammer behavior and confirmed some aspects observed during the experimental analysis. By observing experimental data and modeling results using nonlinear tools, the recommendation made to optimize the result was that one should operate with a 0.0 mm gap, because the magnitude of the impact forces was in the same range as the impact force using higher gap values. However, with higher gap values it was observed a nonlinear jump which will demand a careful tuning of the frequencies. The zero gap impact is a robust result.

Acknowledgements The authors wish to thank CNPq and FAPERJ for its support of this research and Dr. Luiz Fernando Franca for his helpful discussions and suggestions.

References

1. Chen, S.: Linear and nonlinear dynamics of drillstrings. Ph.D. thesis, Faculté des Sciences Appliquées, Université de Liège, Liège, Belgium (1995)
2. Dareing, D.W., Deily, F.H., Paff, G.H., Ortloff, J.E., Lynn, R.D.: Downhole measurements of drill string forces and motions. ASME J. Eng. Ind. May, pp. 217–225 (1968)
3. Dykstra, M.W.: Nonlinear drillstring dynamics. Ph.D. thesis, Department of Petroleum Engineering, University of Tulsa, Oklahoma, USA (1996)
4. Cunningham, R.A.: Analysis of downhole measurements of drill string forces and motions. ASME J. Eng. Ind. May, pp. 208–216 (1968)
5. Batako, A.D., Babitsky, V.I., Halliwell, N.A.: A self-excited system for percussive-rotary drilling. J. Sound Vib. **259**, 97–118 (2003)
6. Batako, A.D., Babitsky, V.I., Halliwell, N.A.: Modelling of vibro-impact penetration of self-exciting percussive-rotary drill bit. J. Sound Vib. **271**, 209–225 (2004)
7. Franca, L.F.P., Weber, H.I.: Experimental and numerical study of a new resonance hammer drilling model with drift. Chaos Solitons Fractals **21**, 789–801 (2004)
8. Wiercigroch, M., Neilson, R.D., Player, M.A.: Material removal rate prediction for ultrasonic drilling of hard materials using an impact oscillator approach. Phys. Lett. A **259**, 91–96 (1999)
9. Babitsky, V.I., Kalashnikov, A.N., Meadowsa, A., Wijesundara, A.A.H.P.: Ultrasonically assisted turning of aviation materials. J. Mater. Process. Technol. **132**, 157–167 (2003)
10. Wiercigroch, M., Wojewodab, J., Krivtsov, A.M.: Dynamics of ultrasonic percussive drilling of hard rocks. J. Sound Vib. **280**, 739–757 (2005)
11. Asfar, K.R., Akour, S.N.: Optimization analysis of impact viscous damper for controlling self-excited vibration. J. Vib. Control **11**(1), 103–120 (2005)
12. Peterka, F.: More detail view on the dynamics of the impact damper. Facta Univ. Ser. Mech. Automat. Control Robot. **3**(14), 907–920 (2003)
13. Babitsky, V.I.: Hand-held percussion machine as discrete non-linear converter. J. Sound Vib. **214**, 165–182 (1998)
14. Babitsky, V.I., Krupenin, V.L.: Vibration of Strongly Nonlinear Discontinuous Systems. Springer, Berlin (2001)
15. Mattos, M.C., Weber, H.I.: Some interesting characteristics of a simple autonomous impact system with symmetric clearance. In: ASME—Design Engineering Conference, CD-ROM, 5 pp. (1997)
16. Inman, D.J.: Engineering Vibration. Prentice Hall, New York (1996)
17. Gilardi, G., Sharf, I.: Literature survey of contact dynamics modelling. Mech. Mach. Theory **37**, 1213–1239 (2002)
18. Leine, R.I., Nijmeijer, H.: Dynamics and Bifurcations of Non-Smooth Mechanical Systems. Springer, Berlin (2004)
19. Leine, R.I., van Campen, D.H., van de Vrande, B.L.: Bifurcations in nonlinear discontinuous systems. Nonlinear Dyn. **23**(2), 105–164 (2000)
20. Divenyi, S., Savi, M.A., Franca, L.F.P., Weber, H.I.: Nonlinear dynamics and chaos in systems with discontinuous support. Shock Vib. **13**, 315–326 (2006)
21. Divenyi, S., Savi, M.A., Franca, L.F.P., Weber, H.I.: Numerical and experimental investigations of the nonlinear dynamics and chaos in non-smooth systems. J. Sound Vib. **301**, 59–73 (2007)
22. Peterka, F., Kotera, T., Cipera, S.: Explanation of appearance and characteristics of intermittency chaos of the impact oscillator. Chaos Solitons Fractals **19**, 1251–1259 (2004)
23. Peterka, F.: More detailed view on the dynamics of the impact damper. Facta Univ. Ser. Mech. Automat. Control Robot. **3**(14), 907–920 (2003)
24. Peterka, F., Blazejczyk-Okolewska, B.: An investigation of the dynamic system with impacts. Chaos Solitons Fractals **9**(8), 1321–1338 (1998)
25. Peterka, F.: Bifurcations and transition phenomena in an impact oscillator. Chaos Solitons Fractals **7**(10), 1635–1647 (1996)
26. Strogatz, S.H.: Nonlinear Dynamics and Chaos. Westview Press, Boulder (2000)

27. Shaw, S.W.: Forced vibrations of a beam with one-sided amplitude constraint: theory and experiment. J. Sound Vib. **99**, 199–212 (1985)
28. Shaw, S.W., Holmes, P.J.: Periodically forced linear oscillator with impacts—chaos and long-period motions. Phys. Rev. Lett. **51**, 623–626 (1983)
29. Ing, J., Pavlovskaia, E., Wiercigroch, M., Banerjee, S.: Experimental study of impact oscillator with one-sided elastic constraint. Philos. Trans. R. Soc. A **366**, 679–704 (2008)
30. Thompson, J.M.T., Bokaian, A.R., Ghaffari, R.: Subharmonic resonances and chaotic motions of a bilinear oscillator. J. Appl. Math. **31**, 207–234 (1983)
31. Piiroinen, P.T., Virgin, L.N., Champneys, A.R.: Chaos and period adding: Experimental and numerical verification of the grazing bifurcation. J. Nonlinear Sci. **14**, 383–404 (2004)
32. Hinrichs, N., Oestreich, M., Popp, K.: Dynamics of oscillators with impact and friction. Chaos Solitons Fractals **8**, 535–558 (1997)
33. Todd, M.D., Virgin, L.N.: An experimental impact oscillator. Chaos Solitons Fractals **8**, 699–715 (1997)
34. Aguiar, R.R.: Experimental investigation and numerical analysis of the vibro-impact phenomenon. D.Sc. thesis, Departamento de Engenharia Mecânica, PUC-Rio, Rio de Janeiro, Brazil (2010)